Chaperone-Mediated Autophagy in the Light of Evolution: Insight from Fish

Laury Lescat,[1] Vincent Véron,[1] Brigitte Mourot,[2] Sandrine Péron,[2] Nathalie Chenais,[2] Karine Dias,[1] Natàlia Riera-Heredia,[1] Florian Beaumatin,[1] Karine Pinel,[1] Muriel Priault,[3,4] Stéphane Panserat,[1] Bénédicte Salin,[3,4,5] Yann Guiguen,[2] Julien Bobe,[2] Amaury Herpin,[†,2,6] and Iban Seiliez [†,1]

[1]Université de Pau et des Pays de l'Adour, E2S UPPA, INRAE, UMR1419 Nutrition Métabolisme et Aquaculture, F-64310 Saint-Pée-sur-Nivelle, France

[2]INRAE, UR1037 Laboratory of Fish Physiology and Genomics, Campus de Beaulieu, Rennes, France

[3]CNRS, IBGC, UMR5095, Bordeaux, France

[4]IBGC, UMR5095, Université de Bordeaux, Bordeaux, France

[5]Service Commun de Microscopie, Université de Bordeaux, Bordeaux, France

[6]State Key Laboratory of Developmental Biology of Freshwater Fish, College of Life Sciences, Hunan Normal University, Changsha, Hunan, P.R. China

[†]These authors contributed equally to this work.

***Corresponding author:** E-mail: iban.seiliez@inrae.fr.

Associate editor: Belinda Chang

Abstract

Chaperone-mediated autophagy (CMA) is a major pathway of lysosomal proteolysis recognized as a key player of the control of numerous cellular functions, and whose defects have been associated with several human pathologies. To date, this cellular function is presumed to be restricted to mammals and birds, due to the absence of an identifiable lysosome-associated membrane protein 2A (LAMP2A), a limiting and essential protein for CMA, in nontetrapod species. However, the recent identification of expressed sequences displaying high homology with mammalian LAMP2A in several fish species challenges that view and suggests that CMA likely appeared earlier during evolution than initially thought. In the present study, we provide a comprehensive picture of the evolutionary history of the *LAMP2* gene in vertebrates and demonstrate that *LAMP2* indeed appeared at the root of the vertebrate lineage. Using a fibroblast cell line from medaka fish (*Oryzias latipes*), we further show that the splice variant *lamp2a* controls, upon long-term starvation, the lysosomal accumulation of a fluorescent reporter commonly used to track CMA in mammalian cells. Finally, to address the physiological role of Lamp2a in fish, we generated knockout medaka for that specific splice variant, and found that these deficient fish exhibit severe alterations in carbohydrate and fat metabolisms, in consistency with existing data in mice deficient for CMA in liver. Altogether, our data provide the first evidence for a CMA-like pathway in fish and bring new perspectives on the use of complementary genetic models, such as zebrafish or medaka, for studying CMA in an evolutionary perspective.

Key words: **autophagy, CMA, chaperone-mediated autophagy, Lamp2a, fish, medaka, evolution.**

Introduction

Autophagy (literally the process of cellular "self-eating") is a widespread and evolutionarily conserved process by which intracellular materials and components are degraded within the lysosomal compartment of eukaryotic cells (Klionsky 2005). This "self-eating" process does not only clean up the cells of intracellular misfolded proteins, damaged organelles, or invading microorganisms but is also an adaptive response for providing nutrients and energy in relation to different stresses (Kroemer et al. 2010). As such, autophagy has been shown to play a key role for the control of cellular homeostasis, and dysregulation of this process is implicated in numerous human diseases, including neurodegenerative or infectious diseases, as well as cancers (Jiang and Mizushima 2014).

Depending on the modalities by which the cytoplasmic material is delivered to the lysosomal lumen, three different autophagic routes have been described in mammals: 1) macroautophagy, 2) chaperone-mediated autophagy (also known as CMA), and 3) microautophagy (Galluzzi et al. 2017). Macroautophagy is by far the best-characterized sub-class of autophagy. It involves the formation of double-membrane organelles, or autophagosomes, which engulf portions of cytoplasm for subsequent degradation via lysosomes. Sequestration of the substrates by the autophagosomes in response to starvation occurs mostly in bulk. However, it is now clear that macroautophagy also contributes to the intracellular homeostasis by selectively degrading cargo materials such as aggregated proteins, damaged mitochondria,

Article

peroxisomes, or invading pathogens (Stolz et al. 2014). CMA is a second complementary autophagic route that involves the direct delivery of cytosolic proteins targeted for degradation to the lysosomes (Kaushik and Cuervo 2018). During this process, cytosolic proteins containing a CMA-targeting motif (KFERQ-related sequences) are first recognized by the chaperone HSPA8/HSC70 (Chiang et al. 1989). This substrate/chaperone complex then docks at the lysosomal membrane through specific binding to the cytosolic tail of the lysosome-associated membrane protein 2A (LAMP2A), the only one of the three spliced isoforms of the *LAMP2* gene that has been shown to be essential and limiting for CMA activity (Cuervo and Dice 1996). After unfolding, substrates subsequently translocate across the lysosomal membrane and are degraded. Finally, microautophagy is another declination of the autophagic catabolism, during which cytoplasmic substrates targeted for degradation are directly taken up by the lysosome (or vacuole in yeast) after invagination of the membrane (Farré and Subramani 2004; Uttenweiler and Mayer 2008). As it is, this third autophagic variation could be either very general, engulfing soluble intracellular components without any distinction, or highly selective, sequestering specific organelles like mitochondria, peroxisomes, or portions of nuclei (Li et al. 2012). Interestingly, a similar mechanism mediating microautophagy-like delivery of cytosolic cargos to lysosomes has been recently observed in late endosomes of murine dendritic cells (Sahu et al. 2011). Proteins harboring the KFERQ motif bind HSC70 and are directed to the endosomal membrane to be subsequently internalized into multivesicular bodies in an endosomal sorting complexes required for transport (ESCRT)-dependent and LAMP2A-independent mechanism. This specific mechanism, now referred as endosomal microautophagy (eMI) has also been reported in *Drosophila melanogaster* (Mukherjee et al. 2016).

It is now clearly established that macro- and microautophagy appeared "early" during the evolution. Indeed, homologous genes of *ATG5*, *ATG7*, *ATG10*, *ATG12*, and *ATG8*, being central to the autophagic process, have been isolated in all eukaryotic model organisms investigated to date (Levine and Klionsky 2004). Genetic but also electron microscopy- and sequence-based evidences for macroautophagy have been found in most of the eukaryotic groups of plants (*Arabidopsis thaliana*), amoebozoa (*Dictyostelium discoideum*), yeasts (*Saccharomyces cerevisiae*, *Pichia pastoris*, *Hansenula polymorpha*, *Pichia methanolica*), and metazoa (*Caenorhabditis elegans*, *Dr. melanogaster*, and *Mus musculus*) (Levine and Klionsky 2004; Rusten et al. 2004; Scott et al. 2004). Similarly, ultrastructural- and genetic-based studies demonstrated the occurrence of an effective microautophagy in yeasts (*S. cerevisiae*, *P. pastoris*, and *Ha. polymorpha*), plants (*Ar. thaliana*) as well as in mammalian cells, although specific data on the latter remains limited (Mijaljica et al. 2011). In contrast, the evolutionary picture of CMA still remains blurry. Indeed and until very recently, the absence of any identifiable LAMP2A outside of the tetrapod clade, led to the paradigm that this cellular function appeared "recently" and was therefore restricted to mammals and birds (Tekirdag and Cuervo 2018). Interestingly, in *Dr. melanogaster*, it has thus been suggested that the newly discovered starvation-inducible eMI could be an ancient form of selective autophagy that might fulfill functions that, in mammals, are shared between eMI and CMA (Mukherjee et al. 2016; Tekirdag and Cuervo 2018). Hence, the evolutionary radiation of the CMA function, in relation to the newly characterized eMI, remains to be investigated outside of the tetrapod clade. A first hint into that direction came with the recent identification of expressed sequences displaying high-sequence homology with the mammalian LAMP2A in several fish species (Lescat et al. 2018), suggesting that CMA likely appeared much earlier during evolution than initially thought.

Here, we shade new light on the evolutionary history of the gene *LAMP2* in vertebrates, notably demonstrating that *LAMP2* appeared after the second round of whole-genome duplication (WGD) that occurred at the root of the vertebrate lineage ~500 Ma. Additionally, using the medaka fish model species (*Oryzias latipes*) we now show that *lamp2a* is ubiquitously expressed during early development as well as in several adult tissues. Although the expression of *lamp2a*, although being a pre-requisite, does not necessarily imply CMA functionality—nor does it give insights into its physiological role—we next addressed the existence of functional CMA or a CMA-like pathway in fish. We therefore transiently transfected medaka fibroblast cells (OLF cell line) with a KFERQ-CMA-targeting motif fused to a photoactivable *mCherry1* reporter, developed to specifically track and evaluate CMA activity in mammalian cells (Koga et al. 2011). Our results show that upon starvation, this KFERQ-CMA reporter accumulates in characteristic *puncta* that colocalize within acidic compartments (lysosomes and/or late endosomes) of the cells. Moreover, being totally dependent on *lamp2a* expression, our sets of experiments strongly support the existence of a functional CMA activity in fish. Finally, we also demonstrate that *lamp2a* knockout medakas exhibit pronounced alterations in hepatic carbohydrate and lipid metabolisms in a physiological readout that is similar to what has been observed in mice with defective hepatic CMA (Schneider et al. 2014). Overall, our results univocally demonstrate that the CMA function is definitively not restricted to mammals and birds. This opens up new avenues on the promising use of fish as pertinent model organisms to investigate CMA function as much as either considering fundamental aspects or evolutionary perspectives on the autophagic routes within the different phyla.

Results

LAMP2 Emerged Concomitantly with the Origin of the Vertebrate Lineage

Homology-based searches in the publicly available RNA-seq databases (PhyloFish), providing comprehensive gene expression data from 23 different ray-finned fish species (Pasquier et al. 2016), resulted in the identification of several contigs displaying high-sequence homology with mammalian LAMP2A (Lescat et al. 2018). These results strongly suggested that the Lamp2a protein was present in fish and therefore could have appeared earlier in evolution than initially

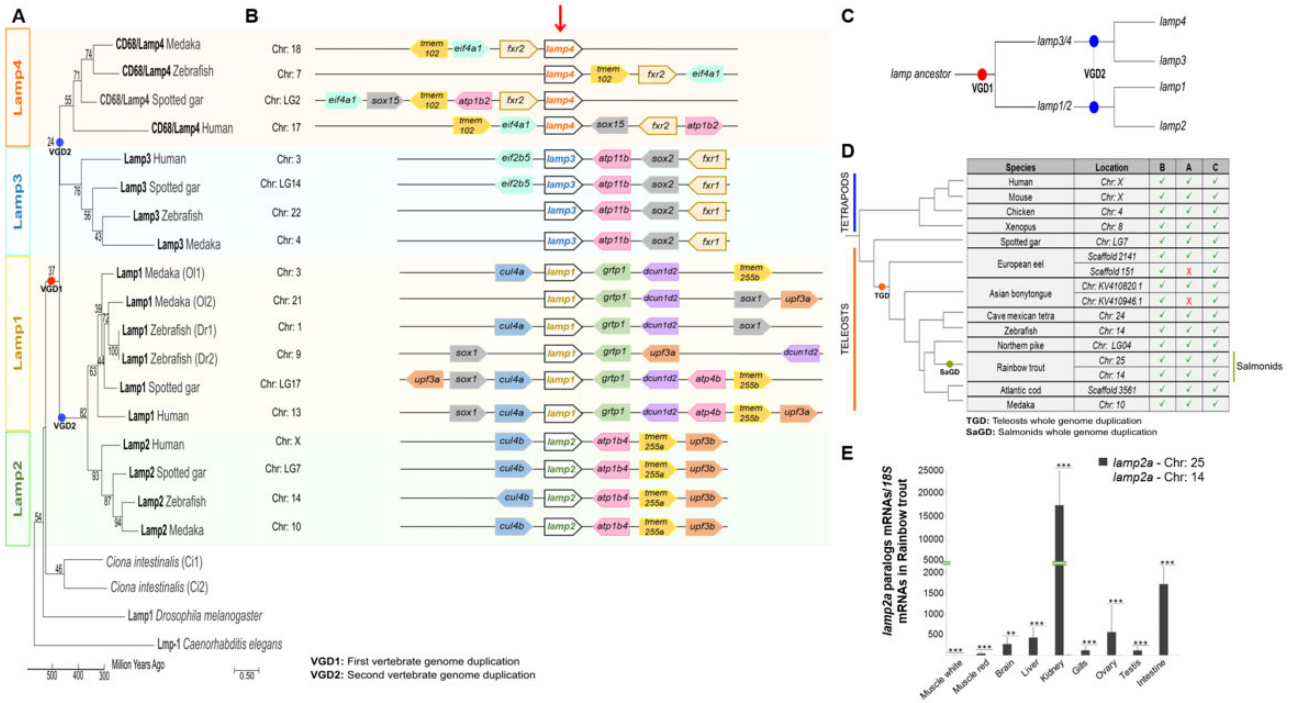

Species	Location	B	A	C
Human	Chr: X	✓	✓	✓
Mouse	Chr: X	✓	✓	✓
Chicken	Chr: 4	✓	✓	✓
Xenopus	Chr: 8	✓	✓	✓
Spotted gar	Chr: LG7	✓	✓	✓
European eel	Scaffold 2141	✓	✓	✓
	Scaffold 151	✓	X	✓
Asian bonytongue	Chr: KV410820.1	✓	✓	✓
	Chr: KV410946.1	✓	X	✓
Cave mexican tetra	Chr: 24	✓	✓	✓
Zebrafish	Chr: 14	✓	✓	✓
Northern pike	Chr: LG04	✓	✓	✓
Rainbow trout	Chr: 25	✓	✓	✓
	Chr: 14	✓	✓	✓
Atlantic cod	Scaffold 3561	✓	✓	✓
Medaka	Chr: 10	✓	✓	✓

FIG. 1. Origin of *lamp2* family gene during evolution. Phylogenetic, syntenic, and genomic organization analyses for the *lamp* family genes in vertebrates. The phylogenetic and syntenic analyses were performed for human (*Homo sapiens*), spotted gar (*Lepisosteus oculatus*), zebrafish (*Danio rerio*), medaka (*Oryzias latipes*), ascidians (*Ciona intestinalis*), fruitfly (*Drosophila melanogaster*), and worm (*Caenorhabditis elegans*). The genomic organization of *lamp2* was analyzed in four tetrapod species and nine fish species. (*A*) Phylogenetic tree, based on full-length amino acid sequences of Lamp1, Lamp2b/a/c (concatenated sequences), Lamp3, and Lamp4 proteins, was built using the maximum likelihood method (the Whelan and Goldman + Freq. model) with 500 bootstrap replicates. The number shown at each branch nodes indicates the bootstrap value (%). The tree was rooted using urochordata and invertebrates Lamp sequences. Accession numbers from Ensembl database are available in supplementary data set S1, Supplementary Material online. (*B*) Genomic synteny compared the orthologs of *lamp* genes and their neighboring genes. Orthologs of each gene are shown in the same color. Genes are represented by block arrows whose directions indicate the gene orientation. The detailed genomic locations of genes displayed in this map are included in supplementary data set S1, Supplementary Material online. (*C*) Schematic scenario of evolutionary history of *lamp* family genes. (*D*) We searched for the presence of the three alternative exons (*B*, *A*, and *C*) in *LAMP2* gene in four tetrapod species—human (*Ho. sapiens*), mouse (*Mus musculus*), chicken (*Gallus gallus*), and frog (*Xenopus tropicalis*), and nine fish species—spotted gar (*L. oculatus*), European eel (*Anguilla anguilla*), Asian bonytongue (*Scleropages formosus*), cave Mexican tetra (*Astyanax mexicanus*), zebrafish (*Da. rerio*), Northern pike (*Esox lucius*), rainbow trout (*Oncorhynchus mykiss*), Atlantic cod (*Gadus morhua*), and medaka (*O. latipes*). The phylogenetic tree is a representative tree of life. The presence or absence of each alternative exon (*B*, *A*, and *C*) is represented by a green check mark or a Red Cross mark, respectively. For each species, the location of the gene is specified in the table. (*E*) Relative expressions of the two *lamp2a* in eight tissues of rainbow trout were determined by RT-qPCR and normalized to *18S* levels. Sets of data are expressed as means + SD ($n = 3$). Nonparametric statistical test pairwise Wilcoxon signed-rank test was performed (*$P < 0.05$, **$P < 0.01$, ***$P < 0.001$).

thought. We therefore sought to further clarify the evolutionary history of the *LAMP2* gene in vertebrates. To this end, phylogenetic analyses have been conducted using sequences of *LAMP* family members (*LAMP1*, *LAMP2*, *LAMP3*, and *LAMP4*/*CD68*/*MACROSIALIN*) including human, three fish species (the zebrafish *Danio rerio*, the medaka *O. latipes*, and the spotted gar *Lepisosteus oculatus*), the urochordate *Ciona intestinalis* and the invertebrates *Dr. melanogaster* and *Ca. elegans* sequences available in Ensembl (Release 96, April 2019). Phylogenetic analyses show that the sequences from the two invertebrates (*Drosophila* and *Ca. elegans*) clustered at the base of the phylogenetic tree (fig. 1*A*). Similarly, the two sequences of the tunicate *Ci. intestinalis* group together outside the subtree of vertebrate *LAMP* genes, suggesting that the apparition of these last genes postdate the divergence of urochordates and vertebrates ~500 Ma. Our phylogenetic analyses also revealed that the fish genomes present at least one ortholog of each human *LAMP* gene. It is worth noting that the WGD that occurred 320–350 Ma in the teleost ancestor (namely, the teleost-specific round of WGD or TGD), theoretically implies that two orthologs (co-orthologs) of each human *LAMP* gene could be present in teleost species, if not lost. Two co-orthologs of the human *LAMP1* (but not of the other *LAMP* genes) were identified in both zebrafish and medaka. In contrast, the spotted gar, whose lineage diverged before the teleost's TGD, exhibits only one *lamp1* (fig. 1*A*).

To further decipher the evolutionary history of *LAMP* genes in vertebrates, synteny analyses were then performed (fig. 1*B* and supplementary fig. S1, Supplementary Material online). High-syntenic conservation was observed between *LAMP1* and *LAMP2* as well as between *LAMP3* and *LAMP4* genomic regions. Paralogous genes were also observed in the vicinity of all *LAMP* genes, reflecting an ancient conserved synteny. Together, these findings strongly suggest that

LAMP genes originated from the first and second rounds of vertebrate WGDs (VGD1 and VGD2) that occurred at the root of the vertebrate lineage. VGD1 resulted in *LAMP1/2* and *LAMP3/4* ancestors (from one *lamp ancestor lamp1/2/3/4*) that subsequently resulted in *LAMP1* and *LAMP2* (from *LAMP1/2*) as well as *LAMP3* and *LAMP4* (from *LAMP3/4*) following VGD2 (fig. 1C).

Overall, our data indicate that *LAMP2* emerged from the second round of WGD that occurred concomitantly with the origin of the vertebrate lineage ~500 Ma, and additionally shows a high conservation of gene synteny in the vicinity of the *LAMP2* locus during vertebrate evolution (supplementary fig. S1, Supplementary Material online).

The Structure of *LAMP2* Is Preserved during the Evolution of Vertebrates

Although it is clearly established that in mammals *LAMP2* contains three alternative splicing forms for its last exon (B, A, and C), encoding the transmembrane domain and cytoplasmic tail specific of each splice variants (*LAMP2B*, *LAMP2A*, and *LAMP2C*, respectively) (Eskelinen et al. 2005), it remained to be determined whether this genomic organization is conserved in other vertebrate taxa, or results from a species- or lineage-specific functional specialization during evolution. To address this question, we next searched for the presence of these three exons in *LAMP2* gene in four tetrapod species (*Homo sapiens*, *M. musculus*, *Gallus gallus*, and *Xenopus tropicalis*) and nine fish with a complete genome sequence available. Our analysis also spans the ray-finned fish tree of life, with special attention for the TGD and the additional and relatively recent salmonid-specific WGD event (salmonid-specific WGD or SaGD), which might have led to significant genomic rearrangements (fig. 1D). Our results show that the four tetrapod genomes contain the three *LAMP2* alternative (B, A, or C) exons (fig. 1D), as does the spotted gar that diverged from the teleost lineage before TGD. Interestingly, both the European eel and the Asian bonytongue, whose lineages diverged shortly after the TGD, have two *lamp2* genes, with one paralog bearing the three alternative exons and the other only the exons B and C. The absence of exon A in the second *lamp2* paralog of these two species, belonging to different super-orders, could result either from independent losses or from the loss of this exon in the common ancestor of teleost shortly after the TGD. However, this second *lamp2* gene, which likely results from the TGD (fig. 1D and supplementary fig. S1, Supplementary Material online), appears to be lost in all other teleost species investigated. Accordingly, in cave Mexican tetra, zebrafish, Northern pike, Atlantic cod, and medaka, a single *lamp2* is found with all three alternative exons (fig. 1D). In rainbow trout, two *lamp2* genes, both exhibiting the three alternative exons A, B, and C, are found. Together with the synteny analysis (supplementary fig. S1, Supplementary Material online), these data suggest that the two rainbow trout *lamp2* genes originated from the WGD event that occurred in the common ancestor of the salmonids (SaGD) ~100 Ma. Interestingly, we were able to detect the expression of only one of the two rainbow trout *lamp2a*, regardless of the tissue analyzed (fig. 1E). This could indicate that in rainbow trout, only one copy is active. Overall, our data show the presence of at least one *LAMP2* gene presenting the three alternative exons B, A, and C in all vertebrates studied, and highlights the high degree of conservation of the genomic structure of this gene during the evolution of vertebrates, despite the important genomic rearrangements these species experienced.

lamp2a Is Ubiquitously Expressed during Early Medaka Development and in Adult Tissues

We next characterized the developmental and tissue-specific expression pattern of the three *lamp2* transcript variants (*lamp2a*, *lamp2b*, and *lamp2c*) in medaka. Results show that the medaka *lamp2b* splice variant transcripts are highly expressed as early as 1-cell stage, and decline slightly during development (fig. 2A). In comparison, *lamp2a* mRNAs are expressed from gastrula stage (stage 13/14), reach a maximum level of expression during the 12–30 somite stages (from stages 23/24 to stages 27/28), before steadily decreasing until hatching stage (stage 39). As for *lamp2c*, although some expression can be detected from gastrula stage (stage 13/14), mRNA levels are much lower than those of the other splice variants. The tissue-specific expression profile of *lamp2a* mRNAs analyzed in adult fish revealed a similar pattern (although not entirely identical) between males and females, with higher levels in gonads, kidneys, liver and, to a lesser extent, brain compared with other tissues (fig. 2B and C). Similarly, *lamp2b* transcript levels were higher in gonads than in other tissues, and *lamp2c* appeared weakly expressed compared with the other two splice variants.

Altogether, our data demonstrate that the specific *lamp2a* splice variant is expressed from the earliest stages of development as well as in different tissues of medaka. Such a dynamic pattern of expression of *lamp2a* (together with that of the two CMA effectors *hsc70/hspa8* and *hsp90aa1*, supplementary fig. S2, Supplementary Material online) de facto suggests that fish might also exhibit CMA activity -or at least a CMA-like process.

Medaka Fibroblast Cell Line Displays CMA Activity

To address the possible function of the newly identified Lamp2a homolog and firmly state on the existence of CMA or a CMA-like pathway in nonmammalian/bird species, we next transiently transfected a medaka fibroblast cell line (OLF) with a photoactivable (PA) KFERQ-PA-mCherry1 fluorescent reporter. This reporter consists of the N-terminal 21 amino acids of bovine RNASE1/RNase A including its KFERQ-CMA targeting motif fused to PA-mCherry. This reporter has previously been used as an in vivo sensor for tracking and estimating CMA activity in mammalian cells upon photoactivation (Koga et al. 2011). In NIH/3T3 mouse fibroblasts, activation of CMA after prolonged starvation induces reporter re-localization from a cytoplasmic diffuse distribution to *puncta* that colocalize with lysosomes (Koga et al. 2011). Here, medaka cells transiently expressing the KFERQ–PA–mCherry1 reporter were photoactivated for 10 min and maintained with (control) or without serum for either 4 or 24 h. In the presence of serum, the reporter appeared diffusely

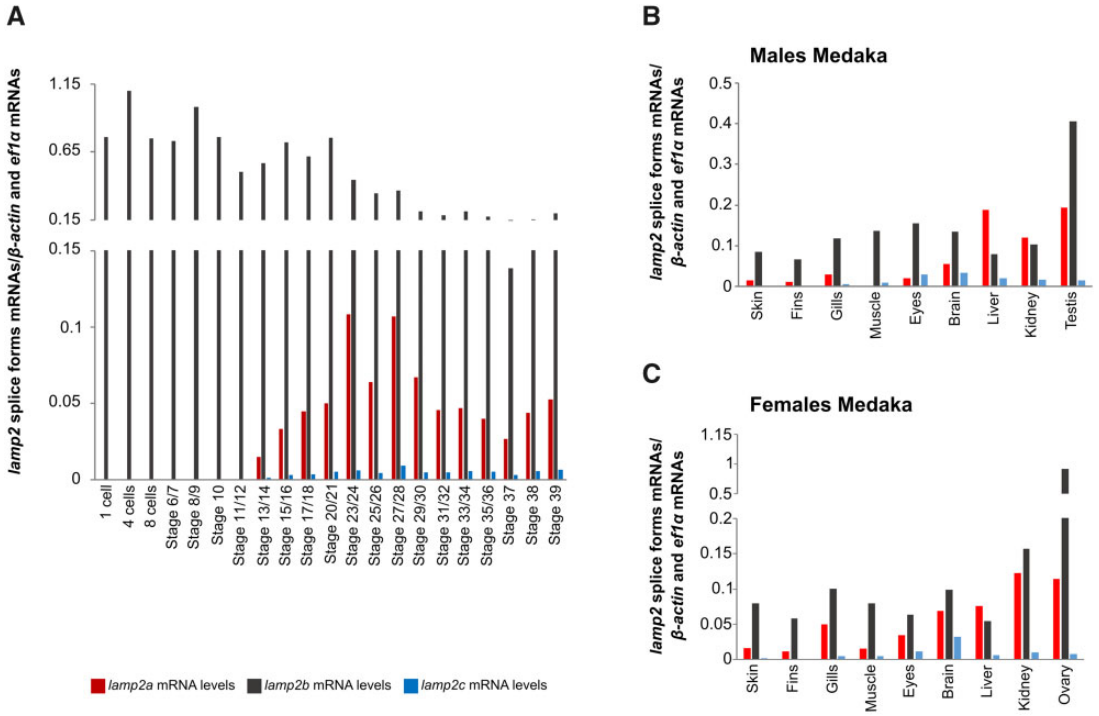

FIG. 2. Expression of the three transcript variants of *lamp2* in medaka during embryonic development and in adult tissues. mRNA levels of *lamp2a*, *lamp2b*, and *lamp2c* were obtained by RT-qPCR in (*A*) embryos at different stages of development and (*B* and *C*) in adult tissues (males and females). Pools of embryos at the same stage ($n = 25$ embryos pooled/stage) or pools of tissues ($n = 5$ fish pooled/tissue) were used. Data are means and were normalized by the values of *β-actin* and *eef1α*.

localized throughout the cytoplasm with only discrete *puncta* sparsely detected (fig. 3A; quantification in fig. 3B). In contrast, after 24 h starvation cells displayed a significantly higher number of KFERQ–PA–mCherry1 *puncta* (fig. 3A; quantification in fig. 3B), colocalizing together with the LysoTracker (fig. 3A; quantification in fig. 3C). Interestingly, after 4 h starvation, when the autophagic flux is already active (supplementary fig. S3, Supplementary Material online), the reporter appeared diffuse throughout the cytosol, indicating that *puncta* formation is kinetically distinct from macroautophagy and dependent on prolonged starvation. Finally, to validate the specificity of our observations and test whether the observed *puncta* indeed require the KFERQ-targeting motif, medaka cells were transfected with a PA–mCherry1 construct lacking the KFERQ motif. Compared with the KFERQ–PA–mCherry1 reporter, the PA–mCherry1 fluorescence remained mainly diffusely localized throughout the cytoplasm and showed very few *puncta*, even after 24-h starvation (fig. 4A; quantification in fig. 4B), demonstrating that the formation of *puncta* depends on the presence of the KFERQ-motif.

In mammals, it has recently been demonstrated that eMI targets proteins also displaying the KFERQ-like motif, but unlike CMA, this process would not require LAMP2A (Sahu et al. 2011). To distinguish between the two systems, it has therefore been proposed to define CMA as an autophagic response that relies specifically on LAMP2A-mediated cargo translocation across the lysosomal membrane (Galluzzi et al. 2017). To determine the mechanisms behind the KFERQ-reporter *puncta* formation observed in OLF cells, the effects of a morpholino (MO)-mediated knockdown of *lamp2a* splicing were tested. Treatment of OLF cells with *lamp2a* MO abolishes specific splicing of *lamp2a* mRNA, while having no significant effect on both *lamp2b* and *lamp2c* splice variants (supplementary fig. S4A, Supplementary Material online). After 24 h starvation, specific knockdown of Lamp2a resulted in a significant loss of KFERQ-reporter *puncta* compared with the 24-h starved control group (fig. 5A; quantification in fig. 5B), while affecting neither the total number nor the activity of the lysosomes in the cells (supplementary fig. S4B and C, Supplementary Material online).

Together, these results clearly support the existence, in a fish cell line, of an autophagic response that, upon long-term fasting specifically targets KFERQ-proteins in a Lamp2a-dependent manner, similarly to the mammalian-defined CMA.

Medaka Lamp2a Mutant (Knockout) Fish Display Severe Alterations of Carbohydrate and Fat Metabolisms

Although the above in vitro results provide a first glimpse accounting for the existence of a functional CMA activity in medaka, the physiological role of this function in this species has so far not been established. In order to address the physiological readout of the presence of a Lamp2a homolog in fish, we generated knockout (Ko) medaka for the specific region corresponding to the *lamp2a* splice variant in the *lamp2* gene, using the genome-editing CRISPR-Cas9 tool (fig. 6A). More specifically, the produced fish displayed a deletion of a 212-bp region in exon 10 of the *lamp2* gene that encodes for the specific cytosolic and transmembrane domains of the Lamp2a protein (fig. 6B and supplementary fig. S5A,

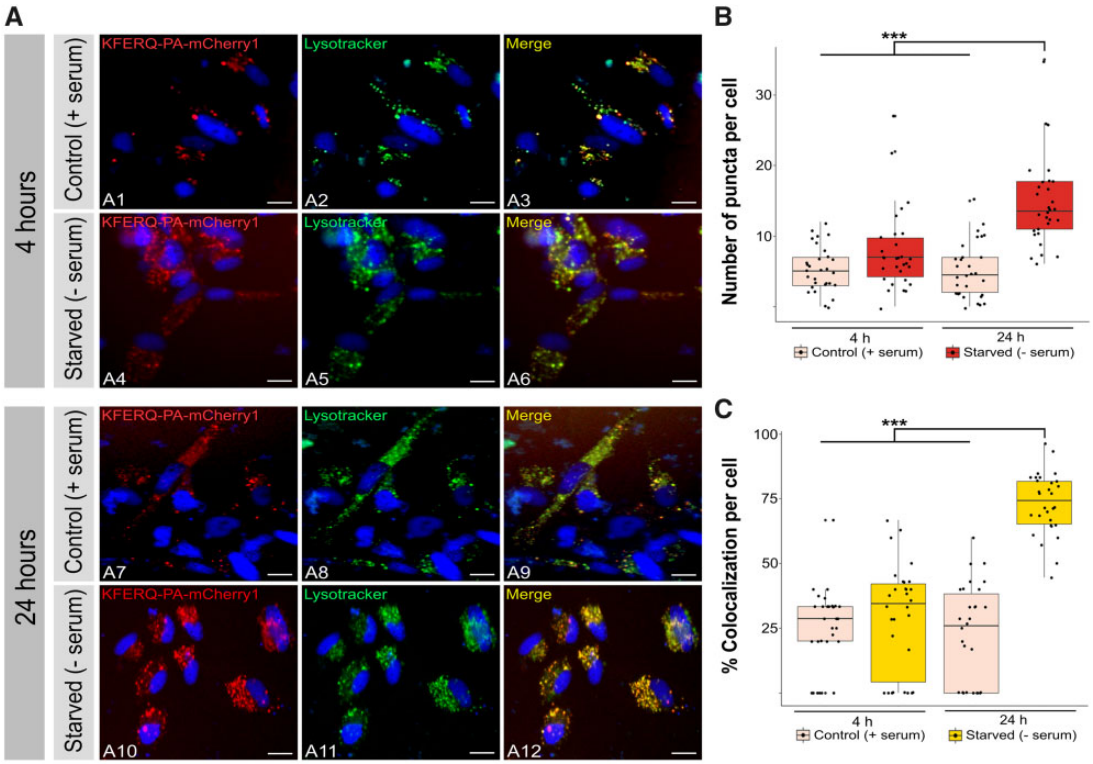

FIG. 3. Relocalization of the fluorescence pattern of the KFERQ-PA-mCherry reporter during starvation in medaka fibroblasts. (*A*) Representative images of medaka fibroblast cells visualized by super-resolution fluorescence microscopy (scale bar, 10 µm). Cells were transfected with a photoactivable (PA) KFERQ-PA-mCherry1 fluorescent reporter (red) and then photoactivated for 10 min. Cells were maintained in the presence or absence of serum for 4 or 24 h. Nuclei were stained with Hoescht 33342 (blue) and lysosomes labeled with Lysotracker (green). (A1–A12) In the presence of serum (Control), the reporter is diffusely localized throughout the cytoplasm with discrete *puncta* rarely detected 4 h (A1–A3) and 24 h (A7–A9) after photoactivation. Under starvation, the reporter is diffusely distributed throughout the cytoplasm after 4 h (A4–A6), but shows a *puncta* pattern after 24 h (A10–A12). (*B*) Quantification of KFERQ-PA-mCherry1 reporter *puncta* per cell under-fed and starved conditions was showed by boxplot. All values are the mean of 30 cells counted for each condition. The ends of the boxes define the 25th and 75th percentiles; a line indicates the median and bars define the 5th and 95th percentiles. Individual values are shown. One-way ANOVA ($P < 0.001$***) was performed with the Tukey post hoc test (*$P < 0.05$, **$P < 0.01$, ***$P < 0.001$). (*C*) Quantification of percentage of colocalization of reporter *puncta* with lysotracker per cell under-fed and starved conditions was showed by boxplot. All values are the mean percentages of 30 cells counted for each condition. Pairwise Wilcoxon signed-rank test was performed with Bonferroni *P* value adjustment (*$P < 0.05$, **$P < 0.01$, ***$P < 0.001$).

Supplementary Material online). Lamp2a knockout medaka (Lamp2a-Ko) were born at Mendelian frequency and proportional male/female ratios were observed for several generations. Levels of *lamp2a* mRNA were undetectable in the tissues of Lamp2a-Ko medaka (fig. 6*C* and supplementary fig. S5*B*, Supplementary Material online), whereas levels of others *lamp2* splice-variants transcripts were comparable with their wild-type counterparts (fig. 6*C* and supplementary fig. S5*B*, Supplementary Material online). Furthermore, transient transfection of primary cell cultures from caudal fins of wild-type and Lamp2a-Ko medaka with the KFERQ-PA-mCherry1 CMA reporter additionally confirmed that cells depleted for Lamp2a no longer exhibit normal CMA activity (supplementary fig. S6*A* and *B*, Supplementary Material online). Interestingly, in agreement with previous reports in mice showing that in vivo blockage of CMA in liver led to a compensatory up-regulation of macroautophagy (Schneider et al. 2015), we similarly observed an induction of steady-state levels of LC3-II, a reliable indicator of autophagosome formation (Klionsky et al. 2016), in the livers of Lamp2a-Ko medaka compared with wild-type fish (fig. 6*D*). These results were further strengthened by an electron microscopy observation, showing that the total number of autophagosome-related vacuoles was significantly more abundant in the liver of mutant fish compared with wild types (supplementary fig. S7, Supplementary Material online).

In light of these results, and considering the critical role(s) of both the CMA and macroautophagy in the control of hepatic metabolism in mammals (Singh et al. 2009; Schneider et al. 2014), we then investigated the metabolic changes induced by the deletion of Lamp2a in medaka. To do so, both Lamp2a-Ko and wild-type fish were subjected to fasting, a procedure known to strongly activate autophagic processes (Cuervo et al. 1995). Figure 6*E* shows that after 16 h of fasting Lamp2a-Ko fish present discrete but significant higher body weight than wild types (fig. 6*E*). Interestingly, Lamp2a-Ko female (but not male) fish also exhibited significantly enlarged livers (fig. 6*F*), suggesting metabolic defects. In this regard, staining of liver sections of Lamp2a-Ko and wild-type fish with the neutral lipid dye oil red O (ORO) revealed higher levels of lipid droplets (LD) in the livers of mutant females (but not males) (fig. 6*G* and supplementary fig.

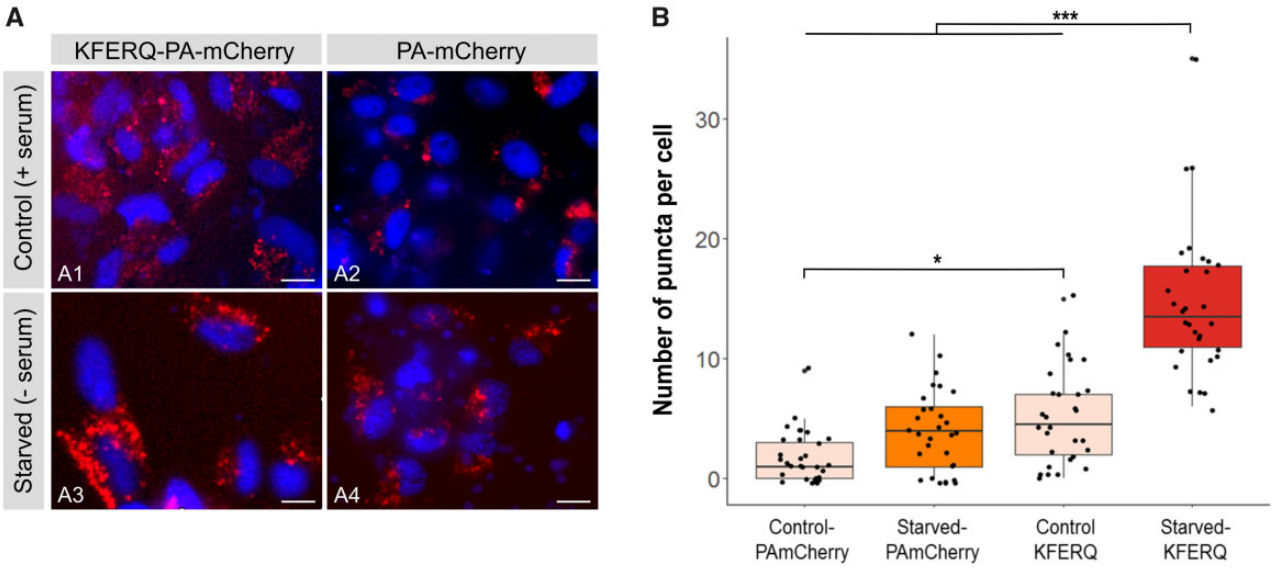

FIG. 4. The presence of the KFERQ-motif is required for the puncta formation. (*A*) Representative images of medaka fibroblast cells visualized by super-resolution fluorescence microscopy (scale bar, 10 μm). Cells were transfected with a photoactivable (PA) KFERQ-PA-mCherry1 red fluorescent reporter or with the photoactivable PA-mCherry1 without the KFERQ motif and then photoactivated for 10 min. Cells were maintained in the presence or absence of serum for 24 h. Nuclei were stained with Hoescht 33342 (blue). The PA-mCherry1 alone is mainly diffused throughout the cytoplasm with rare *puncta* detected even after 24-h starvation. (*B*) Quantification of KFERQ-PA-mCherry1 reporter *puncta* per cell and PA-mCherry1 reporter *puncta* per cell under-fed or starved conditions was shown by boxplot. All values are the mean of 30 cells counted for each condition. The ends of the boxes define the 25th and 75th percentiles; a line indicates the median and bars define the 5th and 95th percentiles. Individual values are shown. One-way ANOVA ($P < 0.001$***) was performed with the Tukey post hoc test (*$P < 0.05$, **$P < 0.01$, ***$P < 0.001$).

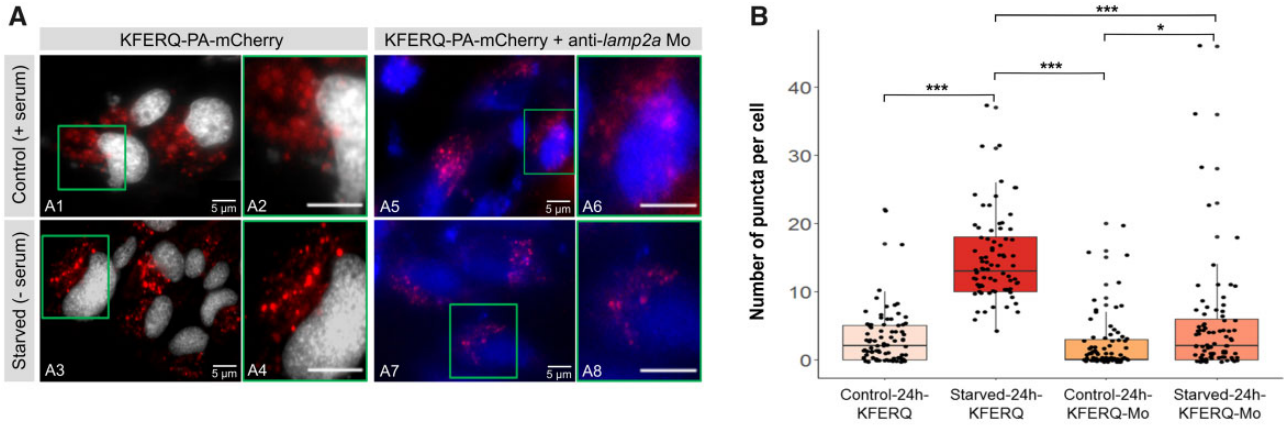

FIG. 5. KFERQ reporter-induced *puncta* formation in medaka cells depends on Lamp2a (*A*) Representative images of medaka fibroblast cells obtained by super-resolution fluorescence microscopy (scale bar, 5 μm). Cells were electroporated with the KFERQ-PA-mCherry1 reporter (red) without (A1–A4) or with (A5–A8) splice-blocking morpholinos against medaka *lamp2a* coupled to a bleu fluorescent tag. Cells were maintained in the presence or absence of serum for 24 h. Nuclei were stained with Hoescht 33342 and visualized in monochrome color (gray) (A1–A4). Enlargement of area boxed in green (A2, A4, A6, and A8). (*B*) Quantification of KFERQ-PA-mCherry reporter red *puncta* per cell was shown by boxplots. After 24-h starvation, specific knockdown of *lamp2a* results in significant losses of KFERQ-reporter *puncta* compared with the 24-h starved control group. All values are the mean of 80 cells for each condition. The ends of the boxes define the 25th and 75th percentiles; a line indicates the median and bars define the 5th and 95th percentiles. Individual values are shown. One-way ANOVA ($P < 0.001$***) was performed with the Tukey post hoc test (*$P < 0.05$, **$P < 0.01$, ***$P < 0.001$).

S8A, Supplementary Material online). Similarly, periodic acid-Schiff (PAS) staining of liver sections showed a slight but significant reduction of glycogen content in livers of Lamp2a-Ko females compared with controls (fig. 6*H* and supplementary fig. S8*B*, Supplementary Material online). Overall, these findings show that loss of Lamp2a function in medaka females leads to severe alterations of carbohydrates and fat metabolisms in the liver, and support the existence of a sexual dimorphism in the role of this gene, at least in medaka.

To determine how Lamp2a deletion led to the observed metabolic perturbations in female medaka, we then analyzed, in liver homogenates of both wild-type and Lamp2a-Ko

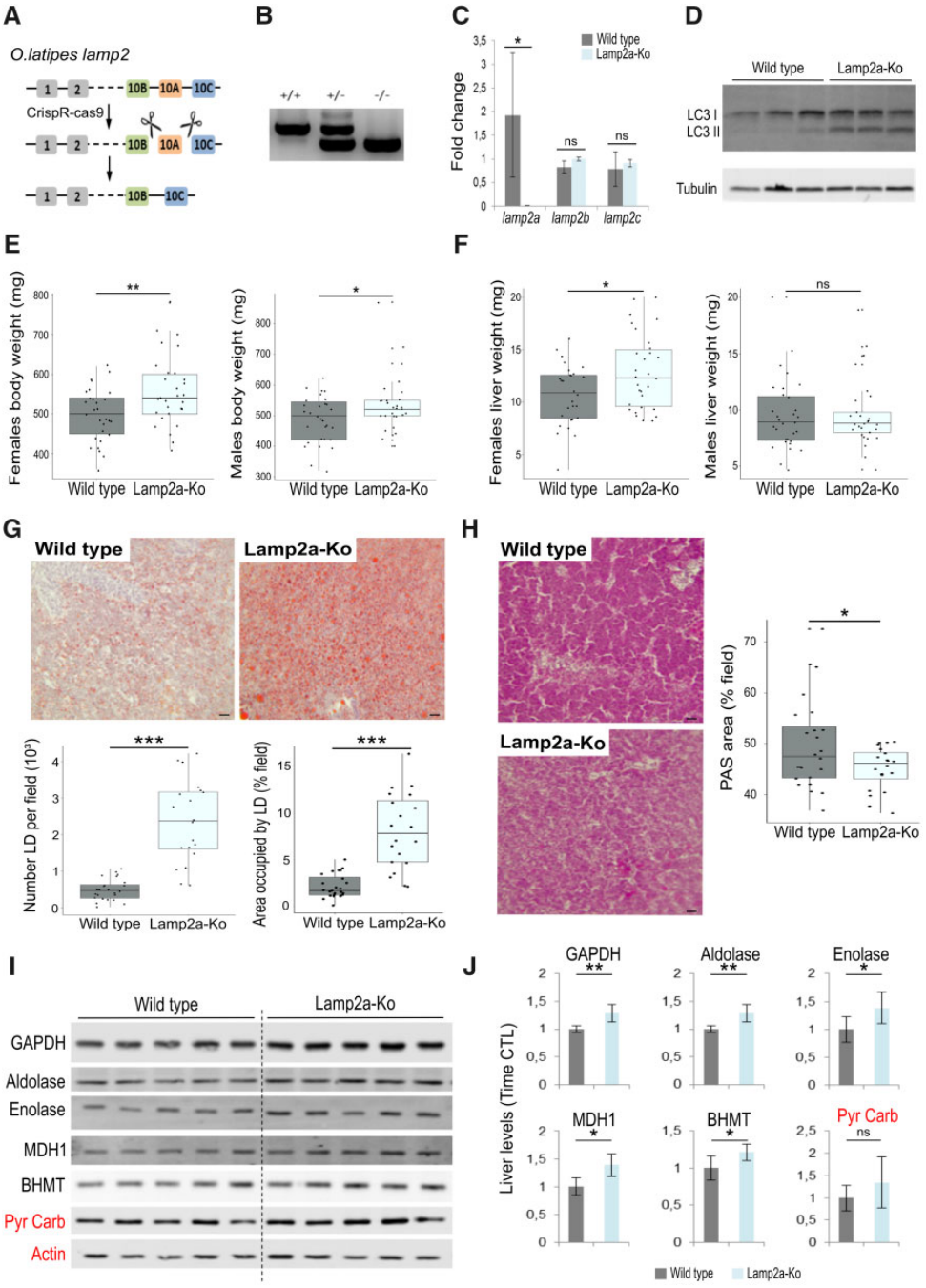

Fig. 6. Lamp2a medaka mutant fish display severe alterations of carbohydrate and fat metabolisms. (*A*) Schematic representation of the strategy used to generate the specific *lamp2a* knockout medaka. (*B*) Genotyping of *lamp2a* allele was performed by PCR of fin fish generated by Crispr-Cas9 method. Mutant fish (−/−) displayed a deletion of the 212 bp (low band) compared with wild-type (+/+) fish (high band). Heterozygous fish (+/−) are shown as an additional control. (*C*) mRNA expression levels were obtained by RT-qPCR in liver from wild-type medaka and Lamp2a-Ko medaka ($n = 3$/condition). Data are means ± SD and were normalized by the values of *eef1α*. (*D*) Representative immunoblot for LC3 I and LC3 II in homogenate liver from wild-type and Lamp2a-Ko medaka. (*E*) Total body weight (mg) of 16-h fasted females and males medaka ($n = 30$/condition). (*F*) Total liver weights (mg) of 16-h fasted females and males medaka ($n = 30$/condition). (*G*) Top: Oil Red O (ORO) staining of liver sections from 16-h fasted wild-type or Lamp2a-Ko female medaka (Scale bar = 20μm). Bottom: quantification of number and area occupied by lipid droplets (LD). For each fish ($n = 6$/condition), four fields were analyzed. (*H*) Left: periodic acid Schiff (PAS) staining of liver sections from 16-h fasted wild-type or Lamp2a-Ko female medaka (Scale bar = 20μm). Right: quantification of area occupied by PAS staining. For each fish ($n = 6$/condition), four fields were analyzed. (*I*) Immunoblot for the indicated enzymes related to carbohydrate and lipid metabolisms in liver homogenates from 24-h fasted wild-type and Lamp2a-Ko females medaka; pyruvate carboxylase (Pyr. Carb) is shown as a negative control. (*J*) Densitometric quantification, values are expressed relative to values in wild-type medaka ($n = 5$–6). GAPDH, glyceraldehyde-3-phosphate dehydrogenase; MDH1, malate dehydrogenase 1; BHMT, betaine-homocysteine S-methyltransferase; Pyr Carb, pyruvate carboxylase. All values are mean ± SD. (*E*–*H*) Parametric statistical test (*t.test*) or (*C* and *J*) nonparametric statistical test (Kruskal–Wallis rank sum test and Wilcoxon signed rank test, respectively) were performed (ns, not significant; $^*P < 0.05$, $^{**}P < 0.01$, $^{***}P < 0.001$).

females, the levels of several enzymes related to carbohydrate and lipid metabolisms and previously reported as bona fide CMA substrates (Schneider et al. 2014). These include enzymes involved in glycolysis (GAPDH, enolase, and aldolase), TCA cycle (MDH1), and lipid stores (BHMT). Immunoblot analysis clearly showed that upon fasting expression levels of these proteins in liver homogenates of Lamp2a-Ko were significantly higher than in wild-type medakas (fig. 6*I* and *J* and supplementary fig. S9, Supplementary Material online). In contrast, pyruvate carboxylase, shown as negative control, did not present any significant difference between Lamp2a-Ko and wild-type fish (fig. 6*I* and *J*). Together, these results suggest that the compromised degradation of these enzymes (involved in glycolysis and lipid stores) might be causal for the observed metabolic perturbations in mutant fish.

Discussion

Recent findings demonstrated that, although most of the "autophagy core" genes are conserved across all eukaryotic species, those coding for proteins involved in the recognition of substrates to be degraded display a rather low conservation in ancient taxa, suggesting a specialization of this function during evolution (Till et al. 2015). Similarly, and due to the failure of identifying *LAMP2A* in genomes other than mammals and birds, functional CMA has long been postulated to be exclusively restricted to a handful of species (Tekirdag and Cuervo 2018). Into that direction it has recently been suggested that the newly discovered starvation-inducible eMI in *Dr. melanogaster* could be an old form of selective autophagy that might fulfill functions that in mammals are shared between eMI and CMA (Mukherjee et al. 2016), again supporting the idea of a "specialization" of the autophagy processes during evolution. Nevertheless, the recent identification of expressed sequences displaying high homology with the mammalian *LAMP2A* in several fish species (Lescat et al. 2018) suggested that CMA likely appeared much earlier during evolution than initially thought.

In order to clarify this issue, we first described the evolutionary history of the *LAMP* family genes in vertebrates. Together, phylogenetic analyses and synteny conservation data strongly suggest that a single copy of *LAMP* was present in the common vertebrate ancestor, and that the successive WGDs (VGD1 and VGD2), that occurred at the root of the vertebrate lineages (Dehal and Boore 2005), resulted in *LAMP1/2* and *LAMP3/4* (from VGD1), then *LAMP1*, *LAMP2*, *LAMP3*, and *LAMP4* (from VGD2) that are common to all vertebrates. Our data also show that despite the significant genomic rearrangements that teleost species experienced (Ravi and Venkatesh 2018), species analyzed in the present study only retained one active copy of the *lamp2* gene carrying the three alternative exons B, A, and C. Interestingly, among all teleost fish species analyzed, salmonid species in which the ancestor experienced a "recent" WGD event ~100 Ma (Berthelot et al. 2014; Macqueen and Johnston 2014), present two *lamp2* genes, each with the three alternative exons B, A, and C, as revealed by our analysis of the rainbow trout genome. However, expression analysis of the two genes suggests that only one of them is actively transcribed, which would be consistent with the pseudogenization of one paralogous copy, a common process following SaGD (Berthelot et al. 2014). These observations are further supported by the recently reported analysis of the PhyloFish RNA-seq database—providing gene expression data from 23 different ray-finned fish species (Pasquier et al. 2016)—revealing the expression of a single *lamp2a* transcript in various salmonid species including rainbow trout but also brook trout (*Salvelinus fontinalis*), brown trout (*Salmo trutta*), grayling (*Thymallus thymallus*), European whitefish (*Coregonus lavaretus*), and American whitefish (*Coregonus clupeaformis*) (Lescat et al. 2018). It is therefore tempting to speculate that loss of expression of the second *lamp2a* transcript has a common origin, probably in the ancestor of salmoniforms shortly after the SaGD. Collectively, these sets of data clearly demonstrate the existence, in a large variety of ray-finned fish species, of an active *lamp2a* splice form and therefore imply that CMA function might have appeared much earlier during evolution than initially thought. Our observations also suggest that evolution tends to favor the presence of a single active Lamp2a protein. Indeed, duplication of the *lamp2* genes following WGD appears to be systematically followed by: 1) the loss of one duplicate, or 2) the loss of the A exon, or 3) the lack of expression of one of the two copies (in the case of the recent SaGD). A single active copy of the *lamp2a* gene appears to be an important feature conserved across vertebrates. This pattern argues for an evolutionary-conserved function of Lamp2a rather than a functional evolution in the different vertebrate lineages.

In order to firmly establish whether or not CMA activity exists in fish, we next transfected a medaka fibroblast cell line with the photoactivable KFERQ-PA-mCherry1 construct, which has proven to be a reliable reporter for tracking and measuring CMA activity in mammalian cells (Koga et al. 2011; Juste and Cuervo 2019). In mammalian NIH/3T3 cells, activation of CMA after prolonged starvation has been shown to induce the re-localization of the KFERQ-PA-mCherry1 reporter from a cytoplasmic diffuse pattern toward *puncta* that colocalize together with lysosomes for subsequent degradation (Koga et al. 2011). In the present study, we provide several lines of evidence for the existence, in a medaka fibroblast cell line, of an autophagic response that upon 24-h fasting specifically targets the KFERQ–PA–mCherry1 reporter to endo-lysosomes (nearly 80% of the *puncta* overlap with the lysotracker that stain acidic compartments in live cells), being consistent with the aforementioned study on mammalian CMA for which this reporter was developed (Koga et al. 2011). However, it has been demonstrated that proteins bearing a KFERQ motif can also be selectively targeted to late endosomes through eMI (Sahu et al. 2011; Mukherjee et al. 2016). Like for CMA, this process requires HSC70 for targeting KFERQ-containing cargo, but in contrast to the former, during which HSC70 binds LAMP2A on lysosomes, cargo delivery by eMI requires HSC70 binding to phosphatidylserines exposed in the outer membrane of endosomes via an ESCRT-dependent and LAMP2A-independent mechanism (Sahu

et al. 2011; Mukherjee et al. 2016). To distinguish both systems, it has therefore been proposed to define the CMA as an autophagic response that relies specifically on LAMP2A-mediated cargo translocation across the lysosomal membrane (Galluzzi et al. 2017). Here, we show that specific knockdown of *lamp2a* in starved medaka fibroblast cells resulted in a significant loss of KFERQ-reporter *puncta*, arguing in favor of a CMA-like process at play in the observed *puncta* instead of eMI. However, it should also be noted that the starved cells in which *lamp2a* was knocked-down still displayed a discrete, but significant, induction of KFERQ-reporter puncta formation compared with their control counterparts. Factually, this might be due either to a residual presence of Lamp2a in the former cells or the existence of a Lamp2a-independent mechanism, for instance, eMI. Considering this later case, such results might indicate that OLF cells show very low ability to target the KFERQ–PA–mCherry1 reporter through eMI, which could be due to either low eMI endogenous activity (at least under the conditions tested) or to the reporter itself that does not bear the protein regions necessary for its targeting by the eMI machinery. Into that direction, it has been shown that although the KFERQ-motif is necessary and sufficient for CMA targeting, in contrast, it is necessary but not sufficient for eMI (Koga et al. 2011). Overall, our findings show for the first time, strong pieces of evidence for a functional CMA or CMA-like process in a fish cell line. Importantly, we also reveal the presence of a CMA or CMA-like activity in cells from caudal fin of wild-type (but not Lamp2a-Ko) medaka, further supporting the existence of this process in fish (and not only in the OLF cell line) and shedding an entirely new light on the evolution of CMA. In the near future, an attractive challenge will be to determine whether—or not—these cells also display significant eMI activity.

Recent studies in mammals demonstrated that CMA plays a key role in hepatic glucose and lipid metabolisms and overall organism energetics (Schneider et al. 2014). Liver-specific knockout for LAMP2A in mice have thus been shown to cause hepatic glycogen depletion and hepatosteatosis together with impaired degradation of key enzymes involved in the use and storage of energy resources (Schneider et al. 2014). Our present study shows that loss of Lamp2a in female medaka leads also to severe alterations of carbohydrates and fat metabolisms in the liver. Precisely, Lamp2a-Ko female fish subjected to a short-term fasting exhibited a marked reduction of hepatic glycogen content as well as pronounced accumulation of lipid droplets compared with the wild-type group. These defects were accompanied by higher levels of enzymes involved in glycolysis (GAPDH, Enolase, Aldolase), TCA cycle (MDH1), and lipid stores (BHMT), suggesting that their compromised degradation is responsible for the observed metabolic disorders in Lamp2a-Ko fish, similarly to what has previously been reported in mice with defective hepatic CMA (Schneider et al. 2014). Thus, our data support that beyond a simple proteolytic system involved in the renewal of obsolete or misfolded proteins, CMA might play, at least in female medaka, a critical role in the control of liver metabolism, by selectively disposing of enzymes involved in several metabolic pathways, as reported in mammals. However, interestingly, this effect of Lamp2a depletion regarding to the levels of metabolic enzymes in liver homogenates is not -or only slightly apparent in fed animals, but only appreciable upon fasting, supporting an involvement of CMA in the adaptation of the metabolism to fasting, through the modulation of the composition of the subproteome directly involved in the use and storage of energy resources. Nevertheless, it should be noted that the deletion of *lamp2a* in males did not lead to any noticeable metabolic alteration, suggesting the existence of functional sex differences at least in medaka. This finding thus provides new exciting avenues for CMA research that should be further explored in the future.

Materials and Methods

Gene and Protein Nomenclature

The nomenclature of genes and proteins is in accordance with the recommendations of the HUGO Gene Nomenclature Committee (for tetrapod species) and the ZFIN Zebrafish Nomenclature Conventions (for fish species).

Medaka Breeding and Treatments

About 5- or 8-month-old male and female CAB medaka (*O. latipes*), wild-type or knockout Lamp2a, were used. Fish were raised at 26 °C under a growing photoperiod (12 h light/12 h dark) and fed with commercial diet three times a day during breeding. Where indicated, fish were starved for 16 or 24 h. For organs sampling, fish were euthanized by immersion in a lethal dose of tricaine (MS-222) at 400 mg/l. All experimental procedures were conducted in strict accordance with the legal frameworks of France and the European Union. They respect the directive 2010/63/EU relating to the protection of animals used for scientific purposes as well as the decree No 2013-118, February 1, 2013 of the French legislation governing the ethical treatment of animals. The protocol was approved by the French National Consultative Ethics Committee under the reference number 10494-2017042809304363.

Establishment of the *lamp2a* Knockout Medaka Line Using *CRISPR/Cas9* Genome Editing

Genome editing of the medaka *lamp2a* splice variant was performed by mean of the CRISPR/Cas9 method according to the protocol described by Herpin et al. (2019). In details, identification of CRISPR/Cas target sites and design of oligonucleotides were performed by the use of the ZiFiT software (http://zifit.partners.org/ZiFiT/Disclaimer.aspx). For preparation of sgRNAs, the DR274 plasmid (Addgene No. 42250) was first linearized with *Bsa1*, electrophoresed in a 2% agarose gel, and purified. Pairs of complementary oligonucleotides were annealed (40 mM Tris–HCl [pH 8.0], 20 mM $MgCl_2$, and 50 mM NaCl buffer) by heating at 95 °C for 2 min and then cooled down slowly to 25 °C within 1 h. The double-stranded oligonucleotides were then ligated into the linearized pDR274 vector. Different sgRNAs were designed to target several intronic sites spanning the *lamp2a* exon in order to create deletions specifically removing the whole 2a exon of the *lamp2* gene. After linearization with *Dra1* and *Not1*,

respectively, pDR274 and pCS2-nCas9n plasmids were used for generating either sgRNAs or *Cas9* RNAs. The synthesized RNAs were then injected into one cell-staged embryos at the following concentrations: 25 ng/µl for each sgRNAs and 100 ng/µl for the *Cas9* mRNA. CRISPR-positive fish were then screened for mutations using PCR primers flanking the site of deletion (supplementary data set S2, Supplementary Material online). Mutant fish used in this study have been outcrossed for at least four generations and always the phenotype observed correlated with the genotype.

Western-Blot Analysis

Livers sampled from wild-type and Lamp2a-Ko medaka were homogenized according to the previously detailed protocol (Belghit et al. 2014). Protein concentrations were determined with the Bradford reagent method (Bradford 1976). Lysates were subjected to SDS-PAGE and immunoblotted using the following antibodies: LC3 (Cell Signaling Technology, No. 3868); GAPDH, glyceraldehyde-3-phosphate dehydrogenase (Cell Signaling Technology, No. 5174); Aldolase (Aviva systems biology, ARP48130); Enolase (Cell Signaling Technology, No. 3810); MDH1, malate dehydrogenase 1 (Aviva systems biology, ARP48283); BHMT, Betaine-Homocysteine S-Methyltransferase (Novus Biologicals, NBP1-55288); Pyr Carb, pyruvate carboxylase (Novus Biologicals, NBP2-33407); and Actin (Santa Cruz Biotechnology, sc-47778). After washing, membranes were incubated with an IRDye infrared secondary antibody (LI-COR Inc, 956-32221). Bands were visualized by Infrared Fluorescence using the Odyssey Imaging System and quantified by Odyssey infrared imaging system software (Application software, version 1.2).

Histology and Electron Microscopy

For oil-red-O (ORO) and periodic acid Schiff (PAS) staining, liver tissue was frozen in OCT, sectioned, and stained with ORO at 0.7% or PAS at 0.5%. Quantification of area occupied by PAS staining and quantification of number and area occupied by lipid droplets (LD) were performed using ImageJ software.

For electron microscopy, fresh liver sampled 16 h after the last meal ($N = 3$/conditions) was fixed with 2.5% glutaraldehyde in 0.1 M phosphate buffer (pH 7.4), and postfixed in 1% osmium tetroxide in phosphate buffer. Conditions of both the treatments of ultrathin sections and observations were already described in Seiliez et al. (2016).

Medaka Fibroblast Cell Line

Oryzias latipes fibroblast (OLF) cell line was from cell bank Riken (RCB0184). They were cultured in home-made ESM4 medium and maintained at 25–26 °C (Yi et al. 2010). ESM4 medium consisted of high-glucose Dulbecco's modified Eagle's medium (DMEM; Invitrogen) supplemented with 20 mM HEPES (Sigma–Aldrich), 15% of FBS clone III (GE Healthcare Life Sciences), 1 embryo/ml of medaka embryo extract (self-prepared), 0.2% of trout serum (self-prepared), 8 ng/ml of human basic fibroblast growth factor (bFGF; PeproTech), 2 mM of L-glutamine (Gibco), 1 mM of nonessential amino acids (Gibco), 1 mM of sodium pyruvate (Gibco), 100 U/ml of penicillin-streptomycin (Sigma), 40 µg/ml of ampicillin (Carl roth), 100 µM of 2-mercaptoethanol (Sigma–Aldrich), and 1 nM of sodium selenite (Sigma–Aldrich), adjusted pH 7.7. Nuclei were labeled using 0.2 mM Hoescht 33342 (ThermoFisher) in mineral medium for 30 min.

Medaka Primary Cells

Caudal fins from wild-type and Lamp2a-Ko medaka (30 fish per group) were collected, washed in PBS containing 10 mg/ml gentamycin and 250 µg/ml amphotericin B. Caudal fins were then minced and digested for 30 min at room temperature in ESM4 containing 2 mg/ml of collagenase (Sigma C2674). Then the mix was filtrated and centrifuged at 150 g for 10 min and the pellet was resuspended in ESM4 medium. Cells were cultivated for 48 h at 25 °C before experimentation.

Construction of the CMA Reporter Plasmid and Anti-*lamp2a* Morpholino Design

The pKFERQ–PA–mCherry1 plasmid was constructed by inserting the oligonucleotide coding for the N-terminal sequence of the bovine ribonuclease A containing the KFERQ-CMA targeting motif (MKETAAAKFERQHMDSSTSAA) (accession number AAB35594) into the *Nhe*I (g/ctagc) and *Bam*HI (g/gatcc) sites of the pPA–mCherry1-N1 vector (addgene), as previously reported in Koga et al. (2011). The primers used were as follows: 5′-aag/ctagcgccaccatgaaggaaactgcagcagc-3′ and 5′-aag/gatccgcagcggaagtgctggagtccatgtgc-3′.

The anti-*lamp2a* morpholino oligonucleotide (5′-GCTGGACAAAGGTGAAAAGAGCAGA-3′) was designed (in collaboration with Gene Tools customer support) to target the splice acceptor site of the exon A of the medaka *lamp2*.

CMA Activity Assay

To track CMA activity, OLF cells or primary cells extracted from wild-type and Lamp2a-Ko medaka were transfected with either the KFERQ-PA-mCherry1 vector or the PA-mCherry1 alone using Xfect transfection reagent (Takara). Transfections were performed from the manufacturer's protocol and adapted to fish cells with incubation for 6 h at 25 °C. The photoactivation was carried out with a 405-nm light source for 10 min and cells were then maintained for 4 or 24 h in the ESM4 medium (serum+) or a serum-free (serum−) mineral medium (132 mM NaCl; 3.1 mM KCl; 1 mM $MgSO_4(7H_2O)$; 1 mM $MgCl_2(6H_2O)$; 3.4 mM $CaCl_2(2H_2O)$; 10 mM HEPES; 1 g/l glucose; 1 g/l pyruvate; pH 8; PO 300mos).

To determine whether the medaka Lamp2a is required for KFERQ-reporter *puncta* formation, OLF cells were electroporated using 1 M buffer (Chicaybam et al. 2013) with KFERQ-PA-mCherry1 vector and the anti-*lamp2a* morpholino (8 µM). Cells were maintained in ESM4 medium (serum+) or mineral medium (serum-) for 24 h. Morpholinos

electroporation was performed by using Nucleofector (Lonza) by following manufacturer's instruction.

Lysosomal Content and Activity in OLF Cells

Acid compartments were labeled in OLF cells by adding 75 nM LysoTracker Green DND-26 (Invitrogen) in the serum-free mineral medium for 30 min. Intracellular lysosomal activity was assessed by loading the cells with the Magic Red Cathepsin B reagent (Bio-Rad) following manufacturer's instructions.

Imaging Procedures

All cells images were acquired in the MRic Photonics platform (Microscopy Rennes imaging center) with DeltaVision Elite high-resolution microscope (GE Healthcare) equipped with a 20× dry and 60× oil objective lens or with Spinning Disk (NIKON Ti-E) equipped with a confocal scanner Unit and a 60× oil objective lens. Quantification of images was done using ImageJ software (National Institutes of Health).

Quantitative RT-PCR Analysis

For qRT-PCR analysis, total RNA was extracted using TRIzol reagent. The protocol conditions for sample preparation and quantitative RT-PCR have been previously published (Seiliez et al. 2016). The primers used for real-time RT-PCR assays are listed in supplementary data set S2, Supplementary Material online. For the expression analysis, relative quantification of target gene expression was done using the ΔCT method described by Pfaffl et al. (2002). Samples were analyzed in triplicates. Data are represented as the relative expression of the gene of interest to a constant expressed reference gene (ef1α, β-actin, or 18S) or a reference gene index consisting of an average of a set of house-keeping genes (e.g., ef1α and β-actin).

In Silico Analysis

To identify *lamp2a*-related transcript sequences in the spotted gar (*L. oculatus*), medaka (*O. latipes*) and Zebrafish (*Da. rerio*), PhyloFish database (http://phylofish.sigenae.org/index.html) (Pasquier et al. 2016) was used (with BLAST-based search). Amino acids sequences of Lamp1, Lamp2 (*b, a, c*), Lamp3, and Lamp4 for human (*Ho. sapiens*), spotted gar, zebrafish, and medaka were collected from Ensembl database (http://www.ensembl.org/index.html, release 96, April 2019).

The orthologs of the *lamps*-related sequence were also collected for ascidian (*Ci. intestinalis*), fruitfly (*Dr. melanogaster*), and worm (*Ca. elegans*). The sequence of Lamp2 for each species is a concatenated sequence using the three splice variants of the gene. Accession numbers from Ensembl database are available in supplementary data set S1, Supplementary Material online.

Phylogenetic tree, based on full-length amino acid sequences, was built using the maximum likelihood method (based on the Whelan and Goldman + Freq. model) with 500 bootstrap replicates and confirmed by neighbor-joining method and minimum likelihood method (500 bootstrap replicates) (supplementary fig. S10, Supplementary Material online) using the Molecular Evolutionary Genetics Analysis (MEGA) software version 7.0 (Kumar et al. 2016).

Syntenic analyses were produced using PhyloView on the Genomicus v95.01 website (http://www.genomicus.biologie.ens.fr/genomicus-95.01/cgi-bin/search.pl) to confirm the evolutionary history of *Lamp* family genes. Synteny for rainbow trout (*Oncorhynchus mykiss*) was performed using NCBI database (https://www.ncbi.nlm.nih.gov/)

For European eel (*Anguilla anguilla*), a BLAST homology search was used to infer synteny relationships using an eel genome sequenced using Oxford Nanopore long reads (Jansen et al. 2017). Accession numbers for synteny analyses are available in supplementary data sets S1 and S3, Supplementary Material online.

Statistical Analysis

All data are reported as means ± SD or means of percentage ± SD. Percentage data have undergone ArcSinus transformation before use. Normality of data residuals was verified before performing parametric or nonparametric statistical tests. For comparisons of more than two groups, we used two-way ANOVA, one-way ANOVA with a Tukey post hoc test (parametric) or pairwise Wilcoxon signed rank test with Bonferroni *P*-value adjustment (nonparametric). For comparisons between two groups, we used Student's *t* test (parametric) or Kruskal–Wallis rank sum test (nonparametric) and Wilcoxon signed rank test (nonparametric). All statistical analyses were performed using R software with the level of significance at $P < 0.05$.

Supplementary Material

Supplementary data are available at *Molecular Biology and Evolution* online.

Acknowledgments

We thank all members of the Club d'Autophagie Bordelais (CAB) for discussions and helpful suggestions. We also thank C. Duret, A. Patinote, S. Gay, and T. Nguyen (from INRA UR1037 LPGP, Rennes), M. Cluzeaud (from INRA-UPPA UMR1419 NuMeA, Saint Pée sur Nivelle), and X. Pinson and S. Dutertre (from Microscopy Rennes Imaging Center, MRic) for their technical assistance. This research was supported by the INRA "Animal Physiology and Livestock Systems" Division, the French National Research Agency (ANR-17-CE20-0033 "Fish-and-Chap"), and the Doctoral School of Exact Sciences and their Applications (ED211) of the UPPA. N.R.-H received fellowship from the MICIUN (BES-2015-074654).

Author Contributions

J.B., A.H., and I.S. got the funding. L.L., J.B., A.H., and I.S. conceived and planned the study. L.L., V.V., B.M., K.D., N.R., F.B., K.P., S.P., N.C., and M.P. performed the experiments. B.S. carried out the electron microscopy analysis. L.L., A.H., and I.S. analyzed the data. L.L., S.P., A.H., Y.G., J.B., and I.S. discussed the experiments. L.L. and I.S. wrote the original draft of the article. I.S., A.H., S.P., Y.G., F.B., and J.B. reviewed and edited the final

version of the article. I.S. supervised the project and had primary responsibility for final content.

References

Belghit I, Skiba-cassy S, Geurden I, Dias K, Surget A, Kaushik S, Panserat S, Seiliez I. 2014. Dietary methionine availability affects the main factors involved in muscle protein turnover in rainbow trout (*Oncorhynchus mykiss*). *Br J Nutr*. 112(4):493–503.

Berthelot C, Brunet F, Chalopin D, Juanchich A, Bernard M, Noël B, Bento P, Da Silva C, Labadie K, Alberti A, et al. 2014. The rainbow trout genome provides novel insights into evolution after whole-genome duplication in vertebrates. *Nat Commun*. 5(1):3657.

Bradford MM. 1976. A rapid and sensitive method for the quantitation microgram quantities of protein utilizing the principle of protein-dye binding. *Anal Biochem*. 72(1–2):248–254.

Chiang H, Terlecky SR, Plant CP, Dice JF. 1989. A role for a 70-kilodalton heat shock protein in lysosomal degradation of intracellular proteins. *Science* 246:382–385.

Chicaybam L, Sodre AL, Curzio BA, Bonamino MH. 2013. An efficient low cost method for gene transfer to T lymphocytes. *PLoS One* 8(3):e60298.

Cuervo AM, Dice JF. 1996. A receptor for the selective uptake and degradation of proteins by lysosomes. *Science* 273(5274):501–503.

Cuervo AM, Knecht E, Terlecky SR, Dice JF. 1995. Activation of a selective pathway of lysosomal proteolysis in rat liver by prolonged starvation. *Am J Physiol Physiol*. 269(5):C1200–C1208.

Dehal P, Boore JL. 2005. Two rounds of whole genome duplication in the ancestral vertebrate. *PLoS Biol*. 3(10):e314–e1708.

Eskelinen E, Cuervo AM, Taylor MRG, Nishino I, Blum JS, Dice JF, Sandoval IV, Lippincott-schwartz J, August JT, Saftig P. 2005. Unifying nomenclature for the isoforms of the lysosomal membrane protein LAMP-2. *Traffic* 6(11):1058–1061.

Farré J-C, Subramani S. 2004. Peroxisome turnover by micropexophagy: an autophagy-related process. *Trends Cell Biol*. 14(9):515–523.

Galluzzi L, Baehrecke EH, Ballabio A, Boya P, Bravo-San Pedro JM, Cecconi F, Choi AM, Chu CT, Codogno P, Colombo MI, et al. 2017. Molecular definitions of autophagy and related processes. *EMBO J*. 36(13):1811–1836.

Herpin A, Schmidt C, Kneitz S, Gobe C, Regensburger M, Le Cam A, Montfort J, Adolfi MC, Lillesaar C, Wilhelm D, et al. 2019. novel evolutionary conserved mechanism of RNA stability regulates synexpression of primordial germ cell-specific genes prior to the sex-determination stage in medaka. *PLoS Biol*. 17(4):e3000185. A

Jansen HJ, Liem M, Jong-raadsen SA, Dufour S, Weltzien F-A, Swinkels W, Koelewijn A, Palstra AP, Pelster B, Spaink H, et al. 2017. Rapid de novo assembly of the European eel genome from nanopore sequencing reads. *Sci Rep*. 7(1):7213.

Jiang P, Mizushima N. 2014. Autophagy and human diseases. *Cell Res*. 24(1):69–79.

Juste YR, Cuervo AM. 2019. Analysis of chaperone-mediated autophagy. In: Ktistakis N, Florey O, editors. Methods in molecular biology. Vol. 1880. New York: Humana Press. p. 703–727.

Kaushik S, Cuervo AM. 2018. The coming of age of chaperone-mediated autophagy. *Nat Rev Mol Cell Biol*. 19(6):365–381.

Klionsky DJ. 2005. Autophagy. *Curr Biol*. 15:282.

Klionsky DJ, Abdelmohsen K, Abe A, Abedin MJ, Abeliovich H, Acevedo Arozena A, Adachi H, Adams CM, Adams PD, Adeli K, et al. 2016. Guidelines for the use and interpretation of assays for monitoring autophagy (III edition). *Autophagy* 12(1):1–222.

Koga H, Martinez-vicente M, Macian F, Verkhusha VV, Cuervo AM. 2011. A photoconvertible fluorescent reporter to track chaperone-mediated autophagy. *Nat Commun*. 2(1):386.

Kroemer G, Mariño G, Levine B. 2010. Autophagy and the integrated stress response. *Mol Cell*. 40(2):280–293.

Kumar S, Stecher G, Tamura K. 2016. MEGA7: molecular evolutionary genetics analysis version 7. 0 for bigger datasets brief communication. *Mol Biol Evol*. 33(7):1870–1874.

Lescat L, Herpin A, Mourot B, Véron V, Guiguen Y, Bobe J, Seiliez I. 2018. CMA restricted to mammals and birds: myth or reality? *Autophagy* 14(7):1267–1270.

Levine B, Klionsky DJ. 2004. Development by self-digestion: molecular mechanisms and biological functions of autophagy. *Dev Cell*. 6(4):463–477.

Li W, Li J, Bao J. 2012. Microautophagy: lesser-known self-eating. *Cell Mol Life Sci*. 69(7):1125–1136.

Macqueen DJ, Johnston IA. 2014. A well-constrained estimate for the timing of the salmonid whole genome duplication reveals major decoupling from species diversification. *Proc R Soc B Biol B*. 281(1778):20132881.

Mijaljica D, Prescott M, Devenish RJ. 2011. Microautophagy in mammalian cells: revisiting a 40-year-old conundrum. *Autophagy* 7(7):673–682.

Mukherjee A, Patel B, Koga H, Cuervo AM, Jenny A. 2016. Selective endosomal microautophagy is starvation-inducible in Drosophila. *Autophagy* 12(11):1984–1999.

Pasquier J, Cabau C, Nguyen T, Jouanno E, Severac D, Braasch I, Journot L, Pontarotti P, Klopp C, Postlethwait JH, et al. 2016. Gene evolution and gene expression after whole genome duplication in fish: the PhyloFish database. *BMC Genomics* 17(1):368.

Pfaffl MW, Horgan GW, Dempfle L. 2002. Relative expression software tool (REST) for group-wise comparison and statistical analysis of relative expression results in real-time PCR. *Nucleic Acids Res*. 30:e36.

Ravi V, Venkatesh B. 2018. The divergent genomes of teleosts. *Annu Rev Anim Biosci*. 6(1):47–68.

Rusten TE, Lindmo K, Juhasz G, Sass M, Seglen PO, Brech A, Stenmark H. 2004. Programmed autophagy in the Drosophila fat body is induced by ecdysone through regulation of the PI3K pathway. *Dev Cell*. 7(2):179–192.

Sahu R, Kaushik S, Clement CC, Cannizzo ES, Scharf B, Follenzi A, Potolicchio I, Nieves E, Cuervo AM, Santambrogio L. 2011. Microautophagy of cytosolic proteins by late endosomes. *Dev Cell*. 20(1):131–139.

Schneider JL, Suh Y, Cuervo AM. 2014. Deficient chaperone-mediated autophagy in liver leads to metabolic dysregulation. *Cell Metab*. 20(3):417–432.

Schneider JL, Villarroya J, Diaz-Carretero A, Patel B, Urbanska AM, Thi MM, Villarroya F, Santambrogio L, Cuervo AM. 2015. Loss of hepatic chaperone-mediated autophagy accelerates proeostasis failure in aging. *Aging Cell* 14(2):249–264.

Scott RC, Schuldiner O, Neufeld TP. 2004. Role and regulation of starvation-induced autophagy in the Drosophila fat body. *Dev Cell*. 7(2):167–178.

Seiliez I, Belghit I, Gao Y, Skiba-cassy S, Dias K, Cluzeaud M, Remond D, Hafnaoui N, Salin B, Camougrand N, et al. 2016. Looking at the metabolic consequences of the colchicine-based in vivo autophagic flux assay. *Autophagy* 12(2):343–356.

Singh R, Kaushik S, Wang Y, Xiang Y, Novak I, Komatsu M, Tanaka K, Cuervo AM, Czaja MJ. 2009. Autophagy regulates lipid metabolism. *Nature* 458(7242):1131–1135.

Stolz A, Ernst A, Dikic I. 2014. Cargo recognition and trafficking in selective autophagy. *Nat Cell Biol*. 16(6):495–501.

Tekirdag K, Cuervo AM. 2018. Chaperone-mediated autophagy and endosomal microautophagy: jointed by a chaperone. *J Biol Chem*. 293(15):5414–5424.

Till A, Saito R, Merkurjev D, Liu J, Syed GH, Kolnik M, Siddiqui A, Glas M, Scheffler B, Ideker T, et al. 2015. Evolutionary trends and functional anatomy of the human expanded autophagy network. *Autophagy* 11(9):1652–1667.

Uttenweiler A, Mayer A. 2008. Microautophagy in the yeast *Saccharomyces cerevisiae*. In: Methods in molecular biology. Totowa: Humana Press. p. 245–259.

Yi M, Hong N, Hong Y. 2010. Derivation and characterization of haploid embryonic stem cell cultures in medaka fish. *Nat Protoc*. 5(8):1418–1430.